Available online at www.sciencedirect.com
SCIENCE DIRECT®
International Journal of Mass Spectrometry 241 (2005) 295–304
International Journal of Mass Spectrometry
www.elsevier.com/locate/ijms

The alkylethynyl radicals, •C≡C-C_nH_{2n+1} ($n = 1-4$), and their anions

Raj K. Sreeruttun[a], Ponnadurai Ramasami[a,*], Ge Yan[b], Chaitanya S. Wannere[b], Paul v. R. Schleyer[b], Henry F. Schaefer[b]

[a] *Department of Chemistry, Faculty of Science, University of Mauritius, Réduit, Mauritius*
[b] *Center for Computational Chemistry, University of Georgia, Athens, GA 30602, USA*

Received 3 December 2004; accepted 13 December 2004
Available online 6 January 2005

Abstract

Alkyl derivatives of the ethynyl radical ($^{\bullet}C_2H$) have been studied using density functional theory (DFT) with DZP++ basis sets. Adiabatic electron affinities (EA_{ad}) and ZPVE-corrected electron affinities for the alkylethynyl series $^{\bullet}C{\equiv}C\text{-}C_nH_{2n+1}$ ($n = 1$–4) have been computed using six different DFT functionals, i.e., BHLYP, BLYP, B3LYP, BP86, BPW91 and B3PW91. These methods have been carefully calibrated for the prediction of electron affinities [J.C. Rienstra-Kiracofe, G.S. Tschumper, H.F. Schaefer, S. Nandi, G.B. Ellison, Chem. Rev. 102 (2002) 231]. The electron affinity of $^{\bullet}C_2H$ (2.969 ± 0.006 eV) has been compared with that of the alkylethynyl series with an attempt to determine the effect of the alkyl chain length on the electron affinities of the acetylenic species. The predicted electron affinities are 2.70 eV ($^{\bullet}C_2CH_3$, experiment = 2.718 ± 0.008 eV), 2.74 eV ($^{\bullet}C_2C_2H_5$), 2.75 eV ($^{\bullet}C_2$-*n*-C_3H_7), and 2.75 eV ($^{\bullet}C_2$-*n*-C_4H_9).

Keywords: Alkylethynyl radicals and anions; Electron affinity; Vibrational frequencies

1. Introduction

The alkylethynyl radicals ($^{\bullet}C_2R$), where R is an alkyl group or a partially modified alkyl chain, are derivatives of the ethynyl radical ($^{\bullet}C_2H$). In fact, they are terminal acetylenic species resulting from the dissociation of precursors having the form C_mH_nX (X = Cl, Br, CN, $SiMe_3$, H). In the past few decades, there have been a number of studies on the ethynyl radical, not only for its electron affinity (EA) [1–11], but also to obtain its equilibrium geometry [12–14]. Chlorine derivative of $^{\bullet}C_2H$ such as the chloroethynyl radical ($^{\bullet}C_2Cl$) have been studied to understand the presence of an electronegative element on the geometry of the ground state [15], in contrast to the $^{\bullet}C_2H$ radical. As a result, it was found that in the ground state, the $^{\bullet}C_2Cl$ radical ($^2A'$ and $^2A'$) is bent, as compared to $^{\bullet}C_2H$ ($^2\Sigma^+$), which is linear [16,17].

The alkylethynyl derivatives have attracted attention in a range of chemical reactions, such as the synthesis of supramolecular complexes [18], antimyotic agents [19] and antihypertensive activity in biological systems [20]. Moreover, the methylethynyl radical, $^{\bullet}C_2CH_3$, is an important molecule in hydrocarbon chemistry [21], in soot formation during combustion [22], and in interstellar chemistry [23].

An interesting point concerning these $^{\bullet}C_2R$ radicals is that their electron affinities are largely unknown, although the electron affinities of $^{\bullet}C_2H$ (2.969 ± 0.006 eV) [1] and $^{\bullet}C_2CH_3$ (2.718 ± 0.008 eV) [24] have been determined. However, there have not been any systematic experimental or theoretical studies to investigate the influence of linear alkyl chains on the electron affinities of the $^{\bullet}C_2R$ radicals.

The present work compares the electron affinity of $^{\bullet}C_2H$ with those of the alkylethynyl radicals. Since it is known [24] that the electron affinity of $^{\bullet}C_2CH_3$ is significantly less than that of $^{\bullet}C_2H$, the longer $^{\bullet}C_2R$ species (R = -C_2H_5, -*n*-C_3H_7, and -*n*-C_4H_9) have been investigated to observe the trend in their electron affinities as the alkyl chain increases. Further,

* Corresponding author.
E-mail addresses: p.ramasami@uom.ac.mu (P. Ramasami), hfs@uga.edu (H.F. Schaefer).

1387-3806/$ – see front matter © 2004 Elsevier B.V. All rights reserved.
doi:10.1016/j.ijms.2004.12.017

Table 1
Theoretical adiabatic electron affinities (eV) for the alkylethynyl radicals predicted from the six different DFT methods with DZP++ basis sets

Alkylethynyl radicals	DFT methods						Experimental values
	BHLYP	BLYP	B3LYP	BP86	BPW91	B3PW91	
$^{\bullet}C_2H$	2.91 (2.92)	2.91 (2.93)	3.13 (3.07)	3.13 (3.10)	2.97 (2.93)	3.02 (3.00)	2.969 ± 0.006 [1]
$^{\bullet}C_2CH_3$	2.60 (2.62)	2.57 (2.55)	2.72 (2.70)	2.74 (2.73)	2.60 (2.58)	2.67 (2.64)	2.718 ± 0.008 [24]
$^{\bullet}C_2C_2H_5$	2.64 (2.67)	2.61 (2.60)	2.76 (2.74)	2.78 (2.78)	2.63 (2.62)	2.71 (2.68)	–
$^{\bullet}C_2$-*n*-C_3H_7	2.65 (2.68)	2.61 (2.60)	2.76 (2.75)	2.79 (2.78)	2.63 (2.63)	2.71 (2.69)	–
$^{\bullet}C_2$-*n*-C_4H_9	2.65 (2.68)	2.60 (2.62)	2.77 (2.75)	2.79 (2.80)	2.63 (2.64)	2.71 (2.69)	–

The ZPVE-corrected electron affinities (eV) are listed in parentheses.

the chain effect on the π network of the acetylene group and the electron distributions have also been studied.

2. Theoretical section

All quantum chemical computations in this study were performed with the Gaussian 94 program system [25]. Total energies, equilibrium energies, harmonic vibrational frequencies and ZPVEs of both the alkylethynyl radicals and anions were obtained using six different gradient-corrected density functional methods (BHLYP, BLYP, B3LYP, BP86, BPW91 and B3PW91). The three HF/DFT hybrid methods were: the BHLYP method, which uses Becke's 1988 exchange functional [26] (B) with the Lee, Yang and Parr correlation functional [27] (LYP); B3LYP which uses Becke's three parameter exchange functional [28] with the LYP correlation functional; and the B3PW91 method which uses Becke's three parameter exchange functional with Perdew and Wang's 1991 (PW91) gradient-corrected correlation functional [29]. The other three functionals were: BLYP which uses the B exchange functional with the LYP correlation functional; BP86 which uses the B exchange functional along the correlation treatment of Perdew [30] (P86); and BPW91 which uses the B exchange and the PW91 correlation functional.

All functionals employed a double-ζ basis set with polarization and diffuse functions, denoted as DZP++. This basis set is constructed by augmenting the Huzinaga and Dunning [31,32] set of contracted double-ζ Gaussian functions with one set of p polarization functions for each H atom and one set of five d polarization functions for each C atom (α_p(H) = 0.75, α_d (C) = 0.75). In addition, one set of even-tempered[33] s and p diffuse functions have been added to each C atom. The s or p diffuse function exponents, $\alpha_{diffuse}$, for a given atom were determined by the formula:

$$\alpha_{diffuse} = \frac{1}{2}\left(\frac{\alpha_1}{\alpha_2} + \frac{\alpha_2}{\alpha_3}\right)\alpha_1$$

where α_1 is the smallest, α_2 the second smallest, and α_3 the third smallest Gaussian orbital exponent of the s or p primitive functions of that atom. There are a total of six DZP++ basis functions per H atom and 19 per C atom.

Spin-unrestricted Kohn–Sham orbitals were used for all the quantum chemical computations. Both the radicals and anions were optimized via analytic energy gradients for all the DFT functionals. All the optimizations were conducted under tight convergence criteria. Moreover, the density was converged to 10^{-8}, and those integrals determined analytically were evaluated with an accuracy of at least to ten digits. Numerical integration was done using the default pruned grid in Gaussian 94 consisting of 75 radial shells with 302 angular points per shell.

The adiabatic electron affinities (EA_{ad}) of the alkylethynyl radicals were computed as the differences between the total energies of the geometry-optimized radical and the total energies of the corresponding geometry-optimized anion.

$$EA_{ad} = E(\text{optimized radical}) - E(\text{optimized anion})$$

ZPVE-corrected electron affinities were also determined by adding the corresponding harmonic ZPVE to the total energies of both radical and anion before subtracting the energy of the anion from that of the radical.

$$\text{ZPVE} = [E(\text{optimized radical}) + \text{ZPVE}_{\text{radical}}] - [E(\text{optimized anion}) + \text{ZPVE}_{\text{anion}}]$$

3. Results and discussion

3.1. Electron affinities

The alkylethynyl radicals have predicted electron affinities (2.55–2.80 eV) less than that of ethynyl radical (2.969 ± 0.006 eV) [1]. The numerical values of the EAs of the different alkylethynyl radicals are reported in Table 1. Moreover, Fig. 1 summarizes the ZPVE-corrected elec-

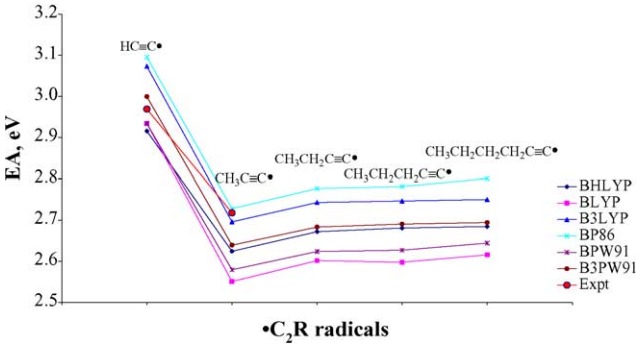

Fig. 1. Effect of chain length on the electron affinities of alkylethynyl radicals.

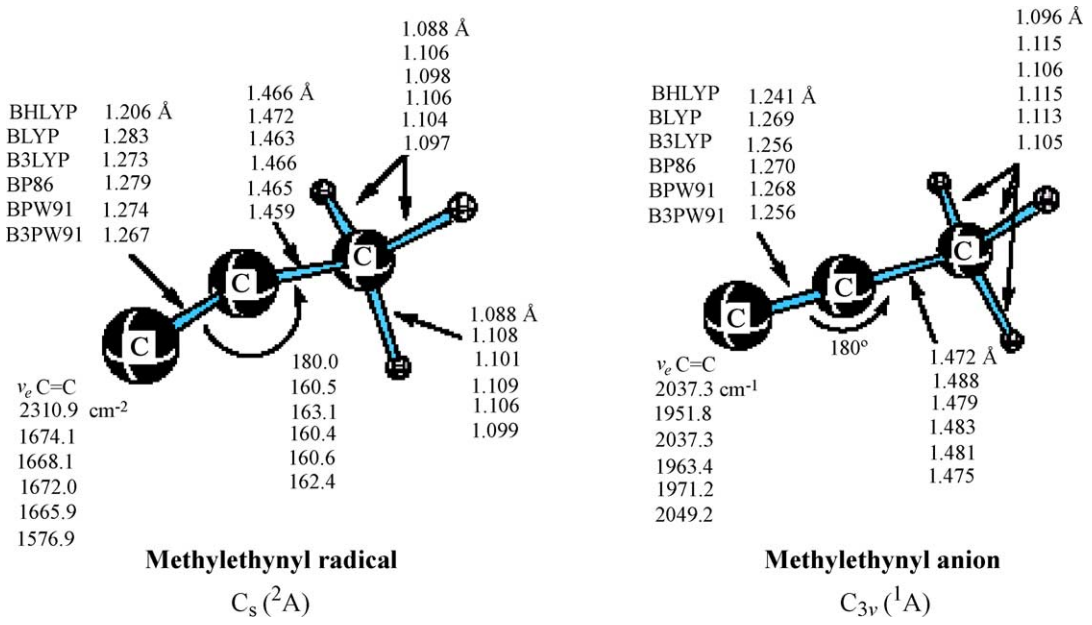

Fig. 2. Equilibrium geometries of methylethynyl radical and anion in the gas phase.

tron affinities with respect to the four different alkylethynyl radicals. It is seen that the six DFT methods have reasonable predicted EA values for the smallest alkylethynyl radicals. The only experimental EA values for the $^{\bullet}C_2R$ (R = H, CH_3) radicals obtained so far are shown in Fig. 1.

The EA values predicted for $^{\bullet}C_2H$ (Experiment = 2.969 ± 0.006 eV) [1] are apparently overestimated by B3LYP (3.07 eV), BP86 (3.10 eV), and B3PW91 (3.00 eV). However, the other functionals underestimate the EA values: BHLYP (2.92 eV), BLYP (2.93 eV) and BPW91 (2.93 eV). Moreover, the experimental EA for $^{\bullet}C_2CH_3$ (2.718 ± 0.008 eV) [24] is very close to the predictions from B3LYP (2.70 eV) and BP86 (2.73 eV). However, BHLYP (2.62 eV), BLYP (2.55 eV), BPW91 (2.58 eV) and B3PW91 (2.64 eV) underestimate the EA values for the $^{\bullet}C_2CH_3$ radical. By and large, the BP86 and B3LYP methods predict better results than the other functionals. Furthermore, for the $^{\bullet}C_2H$ radical, the EA value predicted by these DFT levels is closer to that (3.15 eV) given by the CCSD(T)/DZP++//MP2/DZP++ method.

The electron affinities of the longer alkylethynyl radicals (R = -C_2H_5, -*n*-C_3H_7, and -*n*-C_4H_9) show a slight increase as the alkyl chain length increases.

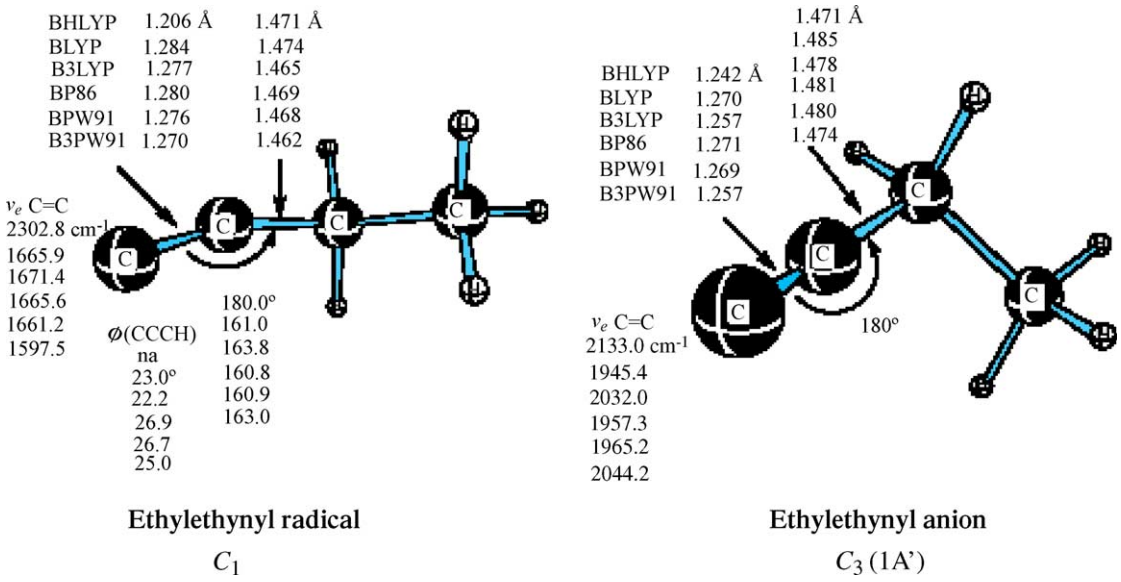

Fig. 3. Equilibrium geometries of ethylethynyl radical and anion in the gas phase.

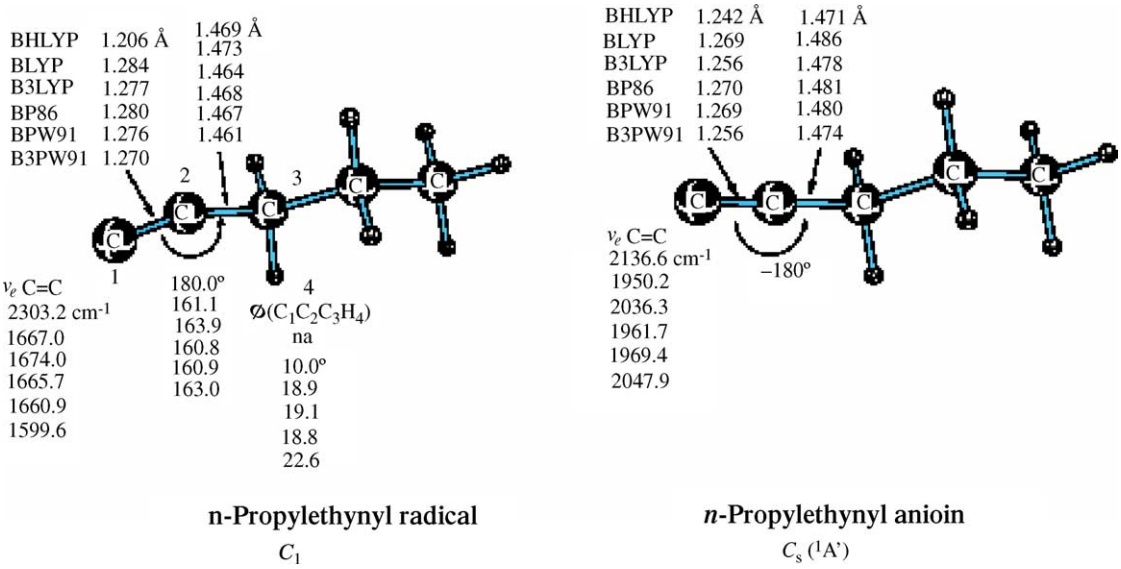

Fig. 4. Equilibrium geometries of *n*-propylethynyl radical and anion in the gas phase.

3.2. Geometries

The optimized geometries of the alkylethynyl species, $^{\bullet}C{\equiv}C\text{-}C_nH_{2n+1}$ ($n = 1-4$), are shown in Figs. 2–5 .

3.2.1. Methylethynyl radical

$^{\bullet}C_2CH_3$ is predicted to have a C_{3v} structure ($^2A_1$) with the MP2/DZP++ method, and the only DFT method that predicts this radical to have a linear C-C≡C frame is BHLYP. The other functionals predict the methylethynyl radical to have C_S symmetry ($^2A'$) in its ground state, with a zero dihedral angle for the CCCH plane. However, the B3LYP method predicts the C_{3v} ($^2A_1$) radical to have an imaginary vibrational frequency for the C-C≡C bending mode, namely 625*i*. The other functionals also compute imaginary frequencies for the C_{3v} ($^2A_1$) radical. For instance, the B3LYP energy difference between the optimized C_S radical and non-optimized C_{3v} radical is predicted to be 2.7 kcal/mol.

3.2.2. Methylethynyl anion

The $^{-}$:C_2CH_3 anion optimizes to a C_{3v} geometry ($^2A_1$) with all functionals.

Table 2
The harmonic vibrational frequencies (cm^{-1}), IR intensities (km/mol) and mode assignments of the methylethynyl radical (C_S) and anion (C_{3v}) predicted by the B3LYP method with DZP++ basis sets

Vibrational mode	Radical				Anion			
	Symmetry	Frequency	IR intensity	Mode assignment	Symmetry	Frequency	IR intensity	Mode assignment
ν_1	A''	137	44	CH_2 rocking	E	288	6	C-C≡C bend
ν_2	A'	332	33	C-C≡C bending	E	288	6	C-C≡C bend
ν_3	A''	815	237	CH_3 wag	A_1	910	7	C-C stretch
ν_4	A'	895	106	CH_3 wag	E	1025	1	CH_2 wag
ν_5	A'	944	42	CH_3 wag	E	1025	1	CH_2 wag
ν_6	A'	1377	9	CH_3 symmetric deformation (in phase)	A_1	1379	37	CH_3 deformation (in phase)
ν_7	A''	1437	40	CH_3 symmetric deformation (out of phase)	E	1470	2	CH_3 deformation (out of phase)
ν_8	A'	1459	16	CH_2 scissors	E	1470	2	CH_2 scissors
ν_9	A'	1669	707	C≡C stretch	A_1	2037	58	C≡C stretch
ν_{10}	A'	3024	1	CH_3 symmetric stretch	A_1	2934	316	CH_3 symmetric stretch
ν_{11}	A'	3091	14	CH_3 antisymmetric stretch	E	2964	99	CH_2 symmetric stretch
ν_{12}	A''	3109	3	CH_2 antisymmetric stretch	E	2964	99	CH_3 antisymmetric stretch

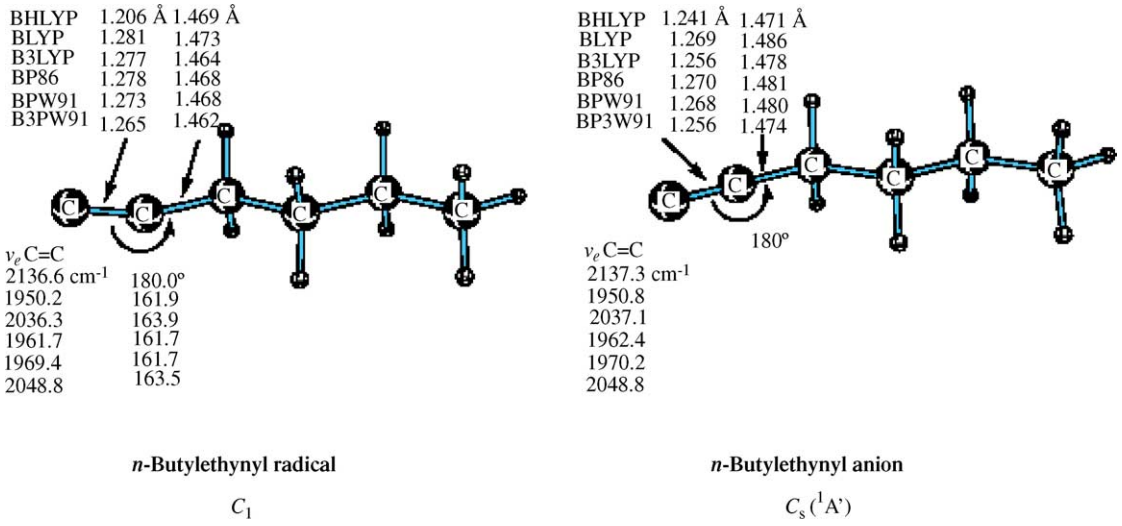

Fig. 5. Equilibrium geometries of *n*-butylethynyl radical and anion in the gas phase.

3.2.3. Ethylethynyl radical

The $^{\bullet}C_2C_2H_5$ radical does not adopt a C_S structure ($^2A'$) with the different functionals, except for BHLYP. Instead, a C_1 symmetry is predicted, as there is bending of the C-C≡C frame (∼160°) and a dihedral angle for the CCCH plane of ∼25°. The same result is observed as compared with the methylethynyl radical. The imaginary vibrational frequency corresponding to C-C≡C bending (C_S structure) with the B3LYP method is 129*i*. Moreover, the energy difference between the C_S constrained radical and the optimized C_1 radical is 0.4 kcal/mol with the B3LYP method.

Table 3
The harmonic vibrational frequencies (cm^{-1}), IR intensities (km/mol) and mode assignments of the ethylethynyl radical (C_1) and anion (C_S) predicted by the B3LYP method with DZP++ basis sets

Vibrational mode	Radical				Anion			
	Symmetry	Frequency	IR intensity	Mode assignment	Symmetry	Frequency	IR intensity	Mode assignment
ν_1	*A*	133	17	≡C-C twist	*A*′	182	5	C-C≡C bend
ν_2	*A*	203	4	CH_3 rock	*A*″	212	0	CH_3 rock
ν_3	*A*	327	38	CH_2 rock	*A*″	314	5	CH_2 rock
ν_4	*A*	396	13	C-C-C bend	*A*′	468	16	C-C-C bend
ν_5	*A*	695	66	CH_2 rock	*A*″	775	0	CH_2 rock
ν_6	*A*	829	2	CH_2 wag	*A*′	822	6	C-H bend
ν_7	*A*	983	56	CH_2 wag	*A*′	1007	10	C-C stretch
ν_8	*A*	1019	3	C-C stretch	*A*′	1068	5	CH_3 wag
ν_9	*A*	1060	17	CH_3 wag	*A*″	1071	1	CH_2 wag
ν_{10}	*A*	1247	16	CH_2 twist	*A*″	1262	0	CH_2 twist
ν_{11}	*A*	1312	75	CH_2 wag	*A*′	1316	63	CH_2 wag
ν_{12}	*A*	1409	1	CH_3 deformation (in phase)	*A*′	1373	7	CH_3 deformation (in phase)
ν_{13}	*A*	1413	65	CH_2 scissors	*A*′	1466	2	CH_2 scissors
ν_{14}	*A*	1488	8	CH_3 deformation (out of plane)	*A*″	1467	3	CH_3 deformation (out of phase)
ν_{15}	*A*	1494	4	CH_2 scissors	*A*′	1490	0	CH_2 scissors
ν_{16}	*A*	1671	613	C≡C stretch	*A*′	2032	112	C≡C stretch
ν_{17}	*A*	3010	7	CH_2 symmetric stretch	*A*′	2930	177	CH_2 symmetric stretch
ν_{18}	*A*	3037	12	CH_2 antisymmetric stretch	*A*″	2943	75	CH_3 antisymmetric stretch
ν_{19}	*A*	3051	27	CH_3 symmetric stretch	*A*′	2980	225	CH_3 symmetric stretch
ν_{20}	*A*	3128	24	CH_3 antisymmetric stretch	*A*′	3067	74	CH_3 antisymmetric stretch
ν_{21}	*A*	3136	22	CH_2 antisymmetric stretch	*A*″	3097	58	CH_2 antisymmetric stretch

Table 4
The harmonic vibrational frequencies (cm^{-1}), IR intensities (km/mol) and mode assignments of the *n*-propylethynyl radical (C_1) and anion (C_S) predicted by the B3LYP method with DZP++ basis sets

Vibrational mode	Radical				Anion			
	Symmetry	Frequency	IR intensity	Mode assignment	Symmetry	Frequency	IR intensity	Mode assignment
ν_1	*A*	92	4	CH_2-CH_2 rock	*A′*	97	10	CH_2-CH_2 torsion
ν_2	*A*	114	20	≡C-C twist	*A′*	148	10	≡C-C bend
ν_3	*A*	243	0	CH_3 rock	*A″*	227	0	CH_3 rock
ν_4	*A*	286	9	C-C-C bend	*A″*	295	4	CH_2 rock
ν_5	*A*	320	43	CH_2 rock	*A′*	324	4	C-C-C bend
ν_6	*A*	404	9	C-C-C bend	*A′*	463	14	C-C≡C bend
ν_7	*A*	685	66	CH_2 rock	*A″*	737	0	CH_2 rock
ν_8	*A*	800	32	CH_2 wag	*A′*	855	8	C-H bend
ν_9	*A*	862	4	CH_3 twist	*A″*	859	2	CH_2 twist
ν_{10}	*A*	948	13	CH_2 wag	*A′*	951	16	≡C-C stretch
ν_{11}	*A*	1030	48	CH_2 twist	*A′*	1037	0	C–C-C antisymmetric stretch
ν_{12}	*A*	1049	5	C-C-C antisymmetric stretch	*A″*	1089	1	CH_2 twist
ν_{13}	*A*	1090	20	C-C stretch	*A′*	1097	1	C-C-C symmetric stretch
ν_{14}	*A*	1225	17	CH_2 twist	*A″*	1234	0	CH_2 twist
ν_{15}	*A*	1261	63	CH_2 wag	*A′*	1275	40	CH_2 wag
ν_{16}	*A*	1306	1	CH_2 twist	*A″*	1292	0	CH_2 twist
ν_{17}	*A*	1370	9	CH_2 wag	*A′*	1352	15	CH_2 wag
ν_{18}	*A*	1410	58	CH_2 scissors	*A′*	1385	4	CH_3 deformation (in phase)
ν_{19}	*A*	1412	2	CH_3 deformation (in phase)	*A′*	1462	1	CH_2 scissors
ν_{20}	*A*	1485	1	CH_2 scissors	*A′*	1479	0	CH_2 scissors
ν_{21}	*A*	1494	8	CH_2 scissors	*A″*	1484	5	CH_2 scissors
ν_{22}	*A*	1500	7	CH_2 scissors	*A′*	1496	5	CH_2 scissors
ν_{23}	*A*	1674	641	C≡C stretch	*A′*	2036	77	C≡C stretch
ν_{24}	*A*	2998	5	CH_2 symmetric stretch	*A′*	2920	193	CH_2 symmetric stretch
ν_{25}	*A*	3026	12	CH_2 antisymmetric stretch	*A″*	2934	61	CH_2 antisymmetric stretch
ν_{26}	*A*	3032	26	CH_3 symmetric stretch	*A′*	3002	87	CH_3 symmetric stretch
ν_{27}	*A*	3053	21	CH_2 symmetric stretch	*A′*	3029	21	CH_2 symmetric stretch
ν_{28}	*A*	3086	1	CH_2 antisymmetric stretch	*A″*	3055	4	CH_2 antisymmetric stretch
ν_{29}	*A*	3110	62	CH_2 antisymmetric stretch	*A′*	3066	95	CH_3 antisymmetric stretch
ν_{30}	*A*	3114	34	CH_3 antisymmetric stretch	*A″*	3082	117	CH_2 antisymmetric stretch

3.2.4. Ethylethynyl anion

All the DFT methods predict the $^-$:$C_2C_2H_5$ anion to have a C_S geometry.

3.2.5. n-Propylethynyl radical

All the DFT methods except BHLYP predict $^\bullet C_2$-*n*-C_3H_7 to adopt a C_1 geometry. The other five functionals consistently show a bending angle of ∼160°. The dihedral angle of the CCCH plane varies from 10 to 23°.

3.2.6. n-Propylethynyl anion

A C_S equilibrium geometry is predicted with all the DFT methods.

3.2.7. n-Butylethynyl radical

$^\bullet C_2$-*n*-C_4H_9 optimizes to a C_1 geometry. An angle of ∼180° is predicted for the C-C≡C frame with the BHLYP method. The other functionals produce a bond angle of ∼160° with a dihedral angle of 16° for the CCCH plane.

Table 5
The harmonic vibrational frequencies (cm^{-1}), IR intensities (km/mol) and mode assignments of the *n*-butylethynyl radical (C_1) and anion (C_S) predicted by the B3LYP method with DZP++ basis sets

Vibrational mode	Radical				Anion			
	Symmetry	Frequency	IR intensity	Mode assignment	Symmetry	Frequency	IR intensity	Mode assignment
ν_1	*A*	82	3	CH_2-CH_2 rock	*A″*	84	10	CH_2-CH_2 torsion
ν_2	*A*	97	17	C-C twist	*A″*	106	0	CH_2 rock
ν_3	*A*	120	2	CH_2 rock	*A′*	116	16	C-C-C bend
ν_4	*A*	205	14	C-C bend	*A″*	233	0	CH_3 rock
ν_5	*A*	243	0	CH_3 rock	*A′*	251	2	C-C≡C bend
ν_6	*A*	318	39	CH_2 rock	*A″*	292	4	C-C≡C bend
ν_7	*A*	371	10	C-C-C bend	*A′*	375	3	C-C-C bend
ν_8	*A*	401	10	C-C-C bend	*A′*	473	15	C-C-C bend
ν_9	*A*	688	79	CH_2 rock	*A″*	730	0	CH_2 rock (in phase)
ν_{10}	*A*	750	16	CH_2 rock	*A′*	785	5	CH_2 rock (out of phase)
ν_{11}	*A*	872	40	CH_2 wag	*A′*	888	4	C-H bend
ν_{12}	*A*	900	11	CH_2 wag	*A″*	919	0	CH_2 twist
ν_{13}	*A*	917	3	CH_2 twist	*A′*	930	1	≡C-C stretch
ν_{14}	*A*	1023	1	C-C stretch	*A′*	1016	2	C-C stretch
ν_{15}	*A*	1049	46	CH_2 twist	*A′*	1055	0	C-C stretch
ν_{16}	*A*	1066	1	C-C antisymmetric stretch	*A″*	1098	21	CH_2 twist
ν_{17}	*A*	1102	12	CH_2 wag	*A′*	1111	1	C-C stretch
ν_{18}	*A*	1214	14	CH_2 twist	*A″*	1222	0	CH_2 twist
ν_{19}	*A*	1241	53	CH_2 wag	*A′*	1250	31	CH_2 wag
ν_{20}	*A*	1290	0	CH_2 twist	*A″*	1287	9	CH_2 twist
ν_{21}	*A*	1317	0	CH_2 twist	*A″*	1299	4	CH_2 twist
ν_{22}	*A*	1334	23	CH_2 wag	*A′*	1331	1	CH_2 wag
ν_{23}	*A*	1393	2	CH_2 wag	*A′*	1372	1	CH_2 wag
ν_{24}	*A*	1410	55	CH_2 scissors	*A′*	1395	6	CH_3 deformation (in phase)
ν_{25}	*A*	1412	2	CH_3 deformation (in phase)	*A′*	1462	1	CH_2 scissors
ν_{26}	*A*	1481	1	CH_2 scissors	*A′*	1474	4	CH_2 scissors
ν_{27}	*A*	1489	0	CH_2 scissors	*A″*	1485	80	CH_3 deformation (out of phase)
ν_{28}	*A*	1493	8	CH_3 deformation (out of phase)	*A′*	1486	186	CH_2 scissors
ν_{29}	*A*	1503	11	CH_2 scissors	*A′*	1499	58	CH_2 scissors
ν_{30}	*A*	1676	656	C≡C stretch	*A′*	2037	51	C≡C stretch
ν_{31}	*A*	2999	5	CH_2 symmetric stretch	*A′*	2921	69	CH_2 symmetric stretch
ν_{32}	*A*	3018	22	CH_2 symmetric stretch	*A″*	2935	56	CH_2 antisymmetric stretch
ν_{33}	*A*	3027	13	CH_2 antisymmetric stretch	*A′*	2998	13	CH_2 symmetric stretch
ν_{34}	*A*	3032	27	CH_3 symmetric stretch	*A′*	3009	69	CH_3 symmetric stretch
ν_{35}	*A*	3044	36	CH_2 symmetric stretch	*A′*	3020	56	CH_2 symmetric stretch
ν_{36}	*A*	3049	11	CH_2 antisymmetric stretch	*A″*	3026	13	CH_2 antisymmetric stretch
ν_{37}	*A*	3090	10	CH_2 antisymmetric stretch	*A″*	3064	39	CH_2 antisymmetric stretch
ν_{38}	*A*	3104	82	CH_2 antisymmetric stretch	*A′*	3071	93	CH_3 antisymmetric stretch
ν_{39}	*A*	3108	44	CH_3 antisymmetric stretch	*A″*	3084	117	CH_2 antisymmetric stretch

3.2.8. n-Butylethynyl anion

A C_S equilibrium geometry is obtained for $^{-}$:C_2-*n*-C_4H_9 after optimization with all the DFT methods. However, there is bending of the C-C≡C frame, while the dihedral angle of the C≡C-C-C plane remains 180°.

Floppiness and quasilinearity are often observed in these alkylethynyl radicals. This may be due to the Jahn–Teller effect. Moreover, the mixing of states or vibronic coupling between the nearby states is one of the plausible causes of such features of the geometries of the radicals.

3.3. Vibrational frequencies and infrared intensities

The theoretical vibrational frequencies of the alkylethynyl radicals and anions are given in Tables 2–5.

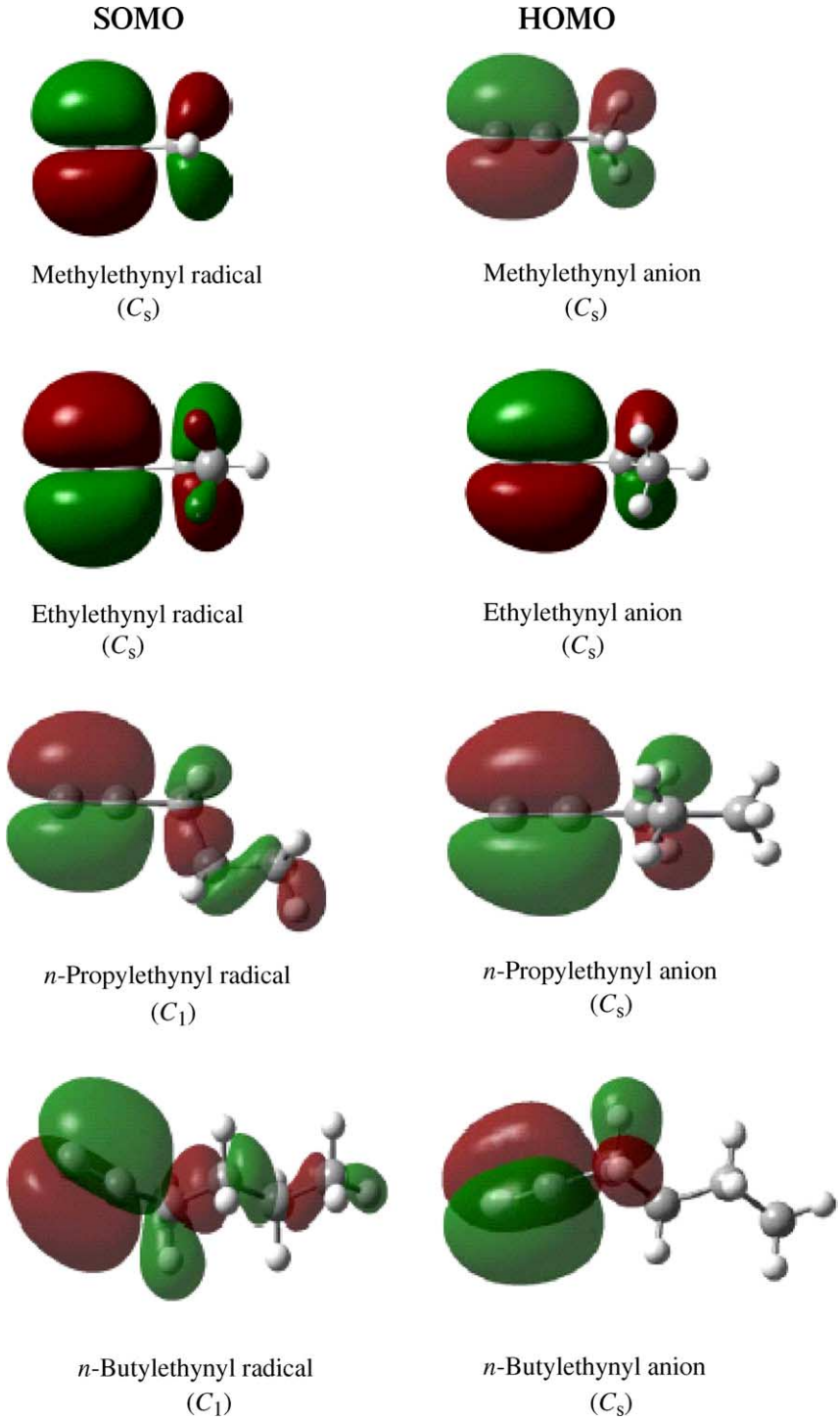

Fig. 6. Plots of the SOMOs and HOMOs of the •C≡CR radicals and the corresponding anions.

The C≡C stretching fundamental for the $^{\bullet}C_2H$ radical is $1850 \pm 20\,cm^{-1}$ [34]. For the alkylethynyl radical derivatives, the C≡C stretch is predicted to be $1669\,cm^{-1}$ ($CH_3C{\equiv}C$), $1671\,cm^{-1}$ ($CH_3CH_2C{\equiv}C$), $1674\,cm^{-1}$ ($CH_3CH_2CH_2C{\equiv}C$), and $1676\,cm^{-1}$ ($CH_3CH_2CH_2CH_2C{\equiv}C$), in a very narrow and nearly arithmetic range. For the anions, the predicted C≡C stretches are $2037\,cm^{-1}$ (methyl), $2032\,cm^{-1}$ (ethyl), $2036\,cm^{-1}$ (propyl), and $2037\,cm^{-1}$ (butyl). These vibrational frequencies show clearly that the $RC{\equiv}C^-$ anions have a tighter C≡C linkage than the $RC{\equiv}C^{\bullet}$ radicals.

3.4. Molecular orbitals

Self-consistent-field (SCF) plots of the molecular orbital of the SOMOs of the radicals and the HOMOs of the anions are illustrated in Fig. 6. The SCF plots have been computed from the optimized geometries predicted by the BH-LYP method. For the radicals, it may be observed that the unpaired electron is delocalized over the carbon–carbon network and this may especially be seen for the longer chains.

The large decrease in EA on going from $^{\bullet}C_2H$ to $^{\bullet}C_2CH_3$ can easily be explained on the basis of the molecular orbitals depicted in Fig. 6. The acetylene anion and its higher analog anions show no qualitative difference in the highest occupied molecular orbital; thus indicating that replacing the H of $^{\bullet}C_2H$ by a methyl group neither stabilizes nor destabilizes the anion HOMO. On the contrary, the SOMO of the respective radicals show significant differences. Since the SOMO and the HOMO of the ethynyl radical and anion, respectively, are localized near the C≡C bond, the EA value of $^{\bullet}C_2H$ is large. However, in the case of only the higher homolog (like methylethynyl) radicals, the unpaired electron is delocalized over the entire molecule. Thus the radical counterparts are more stabilized, which also is reflected in the lower EA values of $CH_3C{\equiv}C^{\bullet}$, etc.

4. Conclusions

The electron affinity of $^{\bullet}C_2H$ is $(2.969 \pm 0.006\,eV)$ [1], notably greater than that of $^{\bullet}C_2CH_3$ $(2.718 \pm 0.008\,eV)$ [24]. As the chain length increases, beyond $^{\bullet}C_2CH_3$ it is observed that the EA values of the $^{\bullet}C_2R$ species increase very slowly. This is due to a *+I* inductive effect which decreases as the alkyl chain length increases. A reasonable explanation of the attenuation of the *+I* effect is that there is a decrease in the electron donating ability of the terminal methyl group as the alkyl chain is lengthened.

Although the radicals are being stabilized by the *+I* effect, the anions are not! The energy gap between the radicals and anions increases, thus causing the EAs to increase very gradually. However, no such effect is seen for the *n*-propylethynyl radical as its EA value remains very similar to that of ethylethynyl radical.

Stabilizing interactions that result from the interaction of the electrons from the σ bonds (C-H bond) with the π system (C≡C), also incline the radicals to have lower energies compared to their respective anions, thus causing the energy gap between the radicals and their respective anions to decrease. In the longer chains this stabilizing effect decreases, causing the electron affinity to increase. The trend is understood from the plot of the radical SOMOs, as there is an interaction of the sigma electrons of the two adjacent C-H bonds with the C≡C network, an interaction commonly known as hyperconjugation.

Acknowledgements

R.K.S. wishes to acknowledge the Tertiary Education Commission (TEC), Mauritius, and the Center for Computational Chemistry (CCC), University of Georgia, Athens, GA 30605, USA, for hosting an extended visit. This research was also supported by the U.S. Department of Energy Combustion Research Program.

References

[1] K.M. Ervin, W.C. Lineberger, J. Chem. Phys. 95 (1991) 1167 (and references therein).
[2] K. Vasudaven, F. Grein, J. Chem. Phys. 68 (1978) 1418.
[3] B.K. Janousek, J.I. Brauman, J. Simons, J. Chem. Phys. 71 (1979) 2057.
[4] J. Baker, R.H. Nobes, L. Radom, J. Comp. Chem. 7 (1986) 349.
[5] W.K. Li, R.H. Nobes, L. Radom, J. Mol. Struc. 149 (1987) 67.
[6] E.G. Lima, S. Canuto, Int. J. Quantum Chem. Symp. 22 (1988) 199.
[7] J.A. Montogomery, G.A. Peterson, Chem. Phys. Lett. 168 (1990) 75.
[8] J. Pacansky, G. Orr, J. Chem. Phys. 67 (1977) 5952.
[9] E.W. David, Chem. Phys. Lett. 244 (1995) 45.
[10] S. Branco, Int. J. Quantum Chem. 72 (1999) 571.
[11] J.C. Rienstra-Kiracofe, G.S. Tschumper, H.F. Schaefer, S. Nandi, G.B. Ellison, Chem. Rev. 102 (2002) 231.
[12] S. Boyé, A. Campos, S. Douin, C. Fellows, D. Gauyacq, N. Shafizadeh, Ph. Halvick, M. Boggio-Pasqua, J. Chem. Phys. 116 (2002) 8843.
[13] W.Y. Chiang, Y.C. Hsu, J. Chem. Phys. 111 (1999) 1454.
[14] Q. Cui., K. Morokuma, J. Chem. Phys. 108 (1998) 626.
[15] Y. Sumiyoshi, T. Ueno, Y. Endo, J. Chem. Phys. 119 (2003) 1426.
[16] D. Forny, M.E. Jacox, J. Thompson, J. Mol. Spect. 170 (1995) 178.
[17] P.G. Szaley, L.S. Thøgersen, J. Olsen, M. Kállay, J. Gauss, J. Phys. Chem. A 108 (2004) 3030.
[18] M. Ochiai, K. Miyamoto, T. Suefuji, M. Shiro, S. Sakamoto, K. Yamaguchi, Tetrahedron 59 (2003) 10153.
[19] G.R. Lovey, A.J. Elliot, General Pharmacology 20, 1989, p. iv (Patent).
[20] J.R. Carson, H.R. Almond, M.D. Brannan, R.J. Carmosin, S.F. Flaim, A. Gill, M.M. Gleason, S.L. Keely, D.W. Ludovici, P.M. Pitis, J. Med. Chem. 31 (1988) 630.
[21] P.R. Wetmoreland, A.M. Dean, J.B. Howard, J.P. Longwell, J. Phys. Chem. 93 (1989) 8171.
[22] U. Alkemade, K.H. Homann, Z. Phys. Chem. 91 (1987) 4455.
[23] P. Thaddeus, J.M. Vrtilek, C.A. Gottlieb, Astrophys. J. 299 (1985) 63.
[24] M.S. Robbinson, M.L. Polak, V.M. Bierbaum, C.H. Depuy, W.C. Lineberger, J. Am. Chem. Soc. 117 (1995) 6766.

[25] M.J. Frisch, G.W. Trucks, H.B. Schlegel, P.M.W. Gill, B.G. Johnson, M.A. Robb, J.R. Cheeseman, K. Raghavachari, M.A. Al-Laham, V.G. Zakrzewski, J.V. Ortiz, J.B. Foresman, J. Cioslwoski, B.B. Stefanov, A. Nanayakkaya, M. Challacombe, C.Y. Peng, P.Y. Ayala, W. Chen, M.W. Wong, J.L. Andres, E.S. Replogle, R. Gomperts, R.L. Martin, D.J. Fox, J.S. Binkley, D.J. Defrees, J. Baker, J.P. Stewart, M. Head-Gordon, C. Gonzalez, J.A. Pople, Gaussian 94, Revision D. 4, Gaussian Inc., Pittsburgh, PA, 1995.
[26] A.D. Becke, J. Chem. Phys. 98 (1993) 1372.
[27] C. Lee, W. Yang, R.G. Parr, Phys. Rev. B 37 (1988) 785.
[28] A.D. Becke, J. Chem. Phys. 98 (1993) 5648.
[29] J.P. Perdew, J.A. Chevary, S.H. Vosko, K.A. Jackson, M.R. Pederson, D.J. Singh, C. Fiolhais, Phys. Rev. B 48 (1993) 4978.
[30] J.P. Perdew, Phys. Rev. B 33 (1986) 8822.
[31] S. Huzinaga, J. Chem. Phys. 42 (1965) 1293.
[32] T.H. Dunning, J. Chem. Phys. 53 (1985) 2823.
[33] T.J. Lee, H.F. Schaefer, J. Chem. Phys. 83 (1985) 1784.
[34] H. Kanamori, K. Seki, E. Hirota, J. Chem. Phys. 87 (1987) 73.